Supplementary Information

Longxing Chi,[1] Chandra Veer Singh,[1,2,] and Jun Nogami,[1,]**

[1]Department of Materials Science and Engineering, University of Toronto, 184 College Street, Toronto, Ontario M5S 3E4, Canada

[2]Department of Mechanical and Industrial Engineering, University of Toronto, 5 King's College Road, Toronto, Ontario M5S 3G8, Canada

Quantum Well States Calculation

The heterostructure created in Figure 3(i) can be approximated to a 1D finite potential well along [120] direction whose energy states can be calculated based on Reference [1]. Given a 1D finite potential well with a well width L and a well depth V_0. The potential energy can be written as:

$$V(x) = \begin{cases} 0, |x| < \frac{L}{2} \\ V_0, |x| > \frac{L}{2} \end{cases}$$

The solution of Schrodinger equation would be

$$\begin{cases} \psi_1(x) = Ae^{\alpha x}, x < -\frac{L}{2} \\ \psi_2(x) = Be^{ikx} + Ce^{-ikx}, |x| < \frac{L}{2} \\ \psi_3(x) = De^{\alpha x}, x > \frac{L}{2} \end{cases}$$

Considering the boundary condition

$\psi_1(-L/2) = \psi_2(-L/2),\ d\psi_1/dx(-L/2) = d\psi_2/dx(-L/2),$

$$\psi_2(L/2) = \psi_3(L/2),\ d\psi_2/dx(L/2) = d\psi_3/dx(L/2),$$

Solving the boundary condition achieves a master equation

$$\sqrt{\frac{m^* L^2 V_0}{2\hbar^2} - v^2} = \begin{cases} v\tan v, & symmetric\ case \\ -v\cot v, & antisymmetric\ case \end{cases}$$

where $v = \frac{kL}{2}$ and m^*, $\hbar$ represent the effective mass and Planck constant, respectively. The master equation can be solved with specific v values at a given m^*, L and V_0. The system energy can then be expressed by

$$E_n = \frac{2\hbar^2 v_n^2}{m^* L^2}$$

In our heterostructure model shown in Figure 3(i). Surface states are considered as valance bands due to the *n*-type Si substrate shitting the Fermi energy (E_F) upwards. Therefore, a well potential of V_0=0.5 eV is used between valance band maximum (VBM) and Fermi energy (E_F). Along [100] direction, the quantum well width is assumed of L=5 nm. The effective hole mass is calculated from our band structure shown in Figures 3(a) and 3(g) at Γ point and from the highest surface state band using

$$\frac{1}{m^*} = \frac{1}{\hbar^2}\frac{d^2E}{dk^2}$$

As calculated effective hole mass m^*=*-1.89*m_e. Therefore, v is calculated from the master equation with eight real solutions v_1=1.45, v_2=2.91, v_3=4.36, v_4=5.80, v_5=7.23, v_6=8.66, v_7=10.06, v_8=11.41. Quantum well states can be calculated as

$$E_n = V_0 - \frac{2\hbar^2 v_n^2}{m^* L^2}$$

The values are E_1=0.49 eV, E_2=0.47 eV, E_3=0.44 eV, E_4=0.39 eV, E_5=0.33 eV, E_6=0.26 eV, E_7=0.17 eV, E_8=0.08 eV. The energy scheme is shown in Figure 3(h).

Tables

Table S1. Bond length

	Bi-Si	Pb-Si	Pb-Bi	Pb-Pb
Bond Length (Å)	2.84	2.71	3.14	3.11
Bond Type	Covalent	Covalent	Covalent	Metallic
Literature value (Å)	2.58~2.83[2-3]	2.66~2.89[4]	3.19~3.78[5-6]	3.14~3.44[7-8]
Bond Type	Covalent	Covalent	--	Metallic

Table S2. Rashba parameter (α_R)

	E_R (eV)	k_0 (Å^{-1})	$\alpha_R=2E_R/k_0$ (eV Å)[9]
Bi in bulk bandgap	0.00188	0.0220	0.171
Pb in bulk bandgap	0.00170	0.0276	0.123
Bi in conduction band	0.023	0.072	0.639

Figures

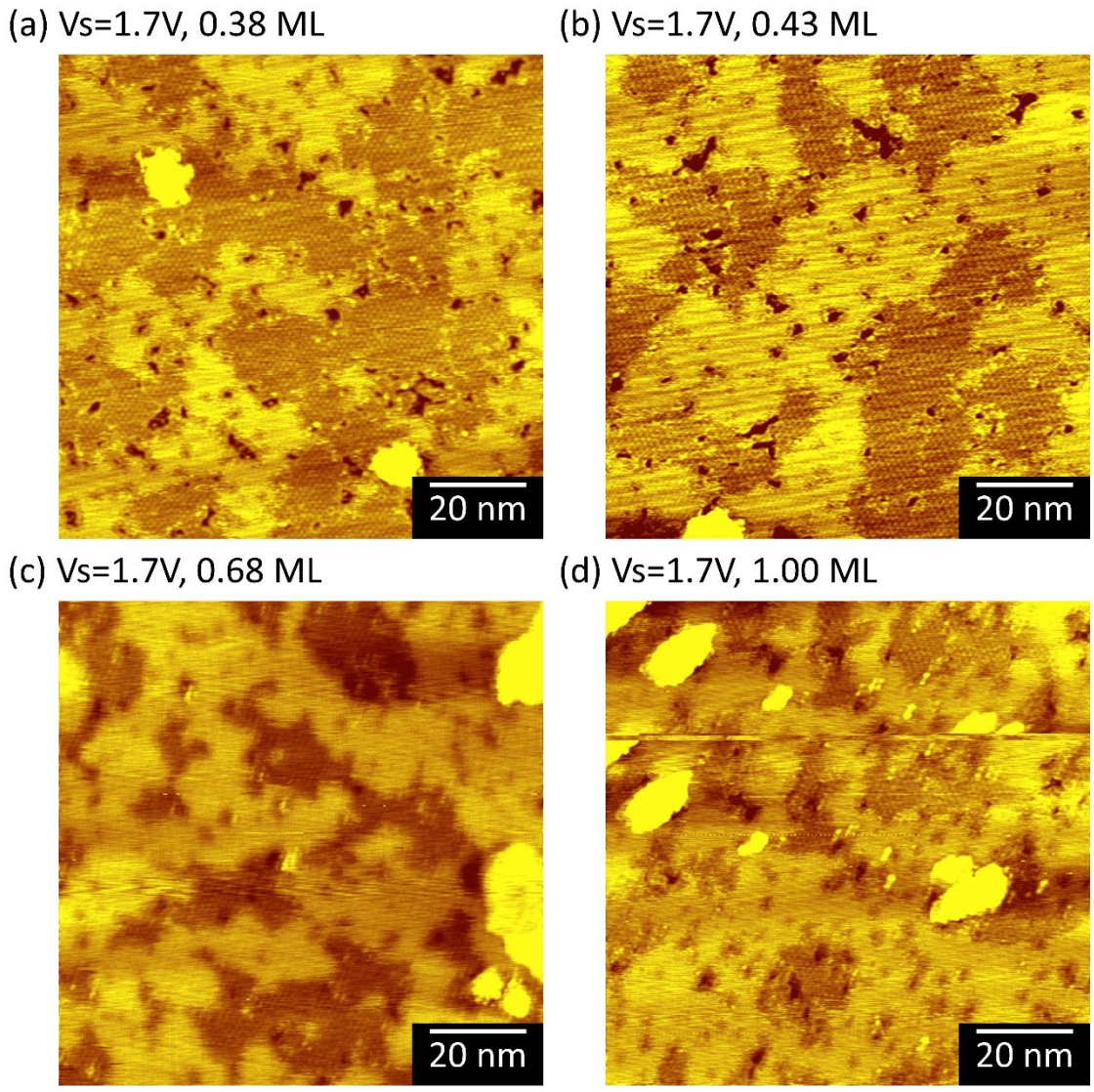

Figure S1. STM images of the $2\sqrt{3}\times2\sqrt{3}$ phase at different Pb coverage. The noisy phase appears at a Pb coverage of 1/3 ML and saturates the surface at 1 ML. Since the noisy phase is not clearly imaged under STM its structure is unknown.

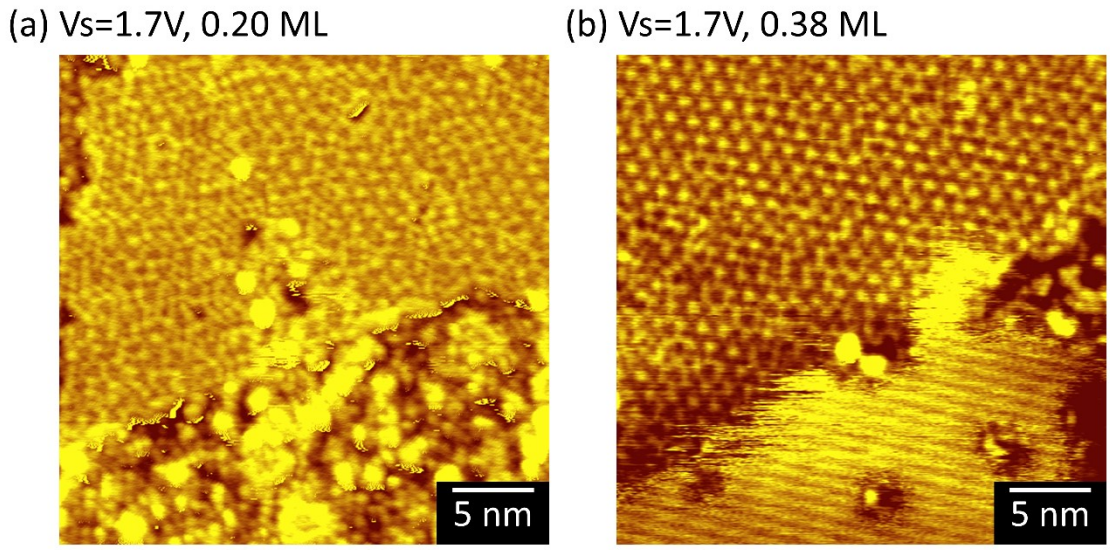

Figure S2. Zoom-in STM images of the 2√3×2√3 phase at different Pb coverage. Lower Pb coverage (0.2 ML) results in higher surface defect density. Accordingly, to achieve a continuous 2√3×2√3 phase, 1/3 ML Pb coverage is necessary, proving that the stoichiometric ratio of Bi to Pb is 1:1.

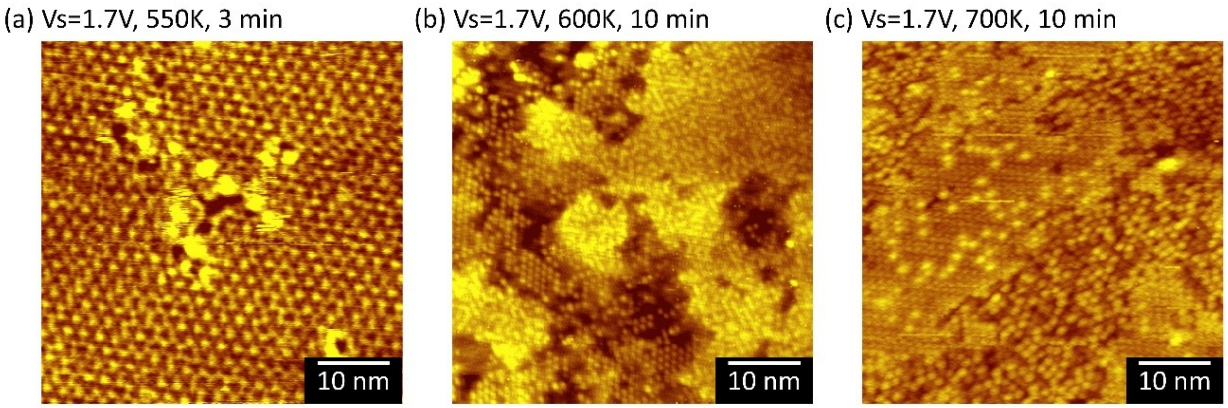

Figure S3. STM images of surfaces under different annealing plans. The $2\sqrt{3}\times2\sqrt{3}$ phase covers the surface at 1/3 ML Pb coverage after annealing at 550K for 3 min. Annealing at 600K for 10 min initiates Pb adatoms dissociation and annealing at 700K for 10 min results in a Pb-free α-phase Bi surface.

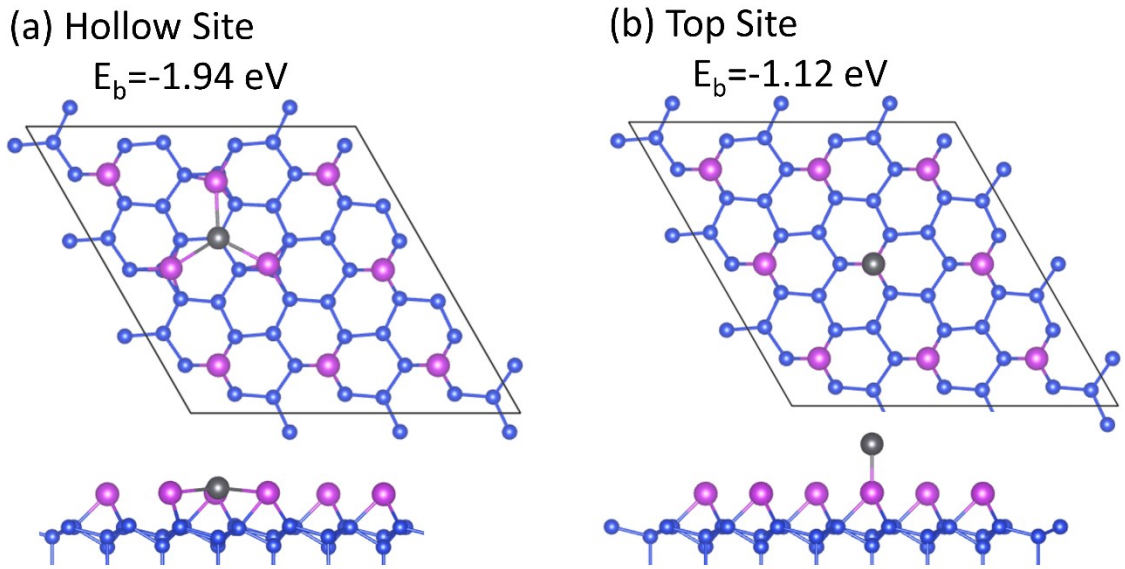

Figure S4. Single Pb adatom adsorption model at hollow site and top site on the α-phase Bi/Si(111) surface. From the calculated adsorption energy, it can be referred that bridge site adsorption is most stable while the top site the least.

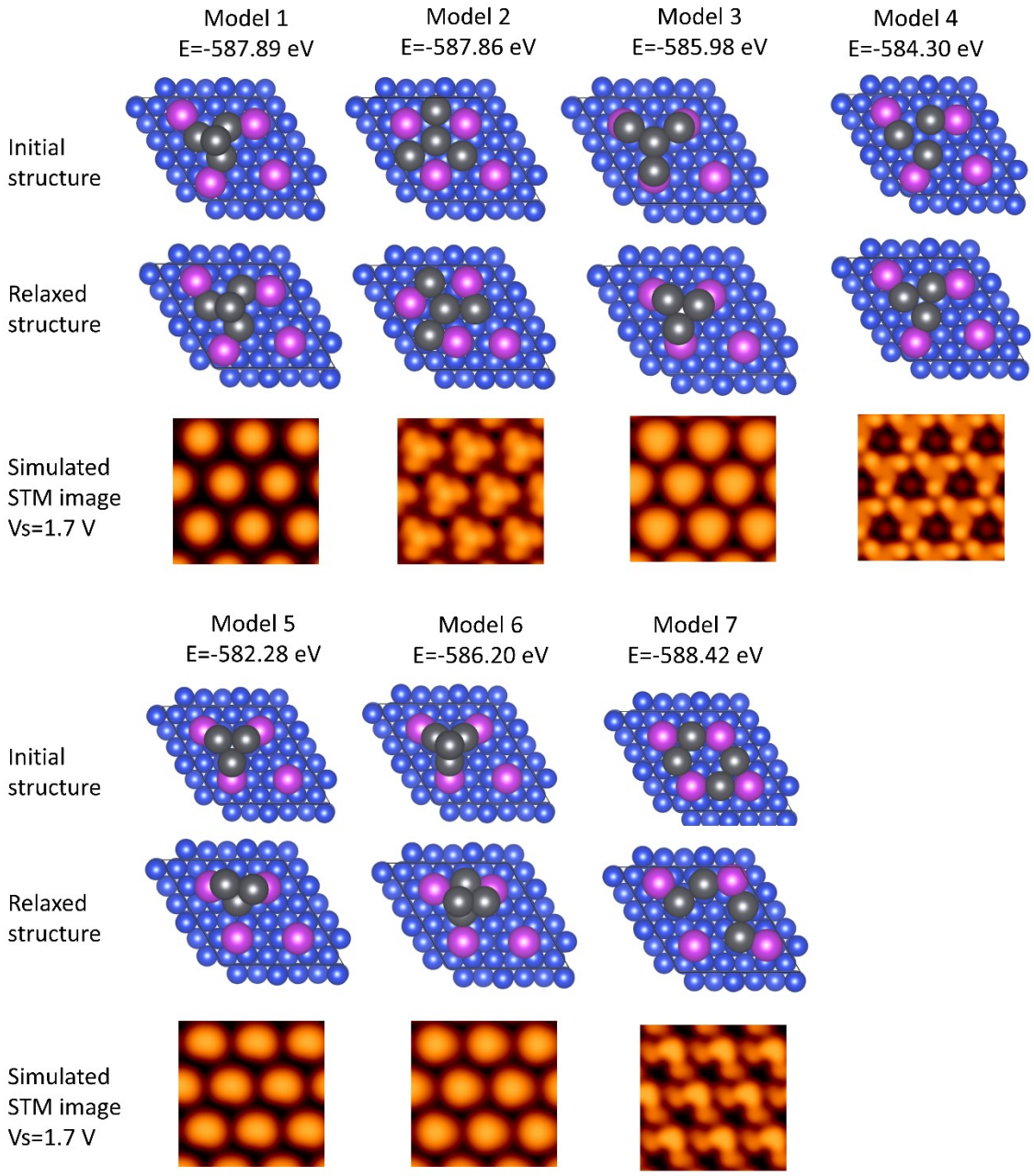

Figure S5. All tested structural models for the $2\sqrt{3}\times2\sqrt{3}$ superlattices. Initial structures shown in first row. Relaxed structures in second row and simulated STM images in third row. Only models 1~3 & 5~6 exhibit a reasonable crystal structure after relaxation and duplicate the real STM images. Therefore, only those models are further examined by *ab initio* molecular dynamics (AIMD) calculation.

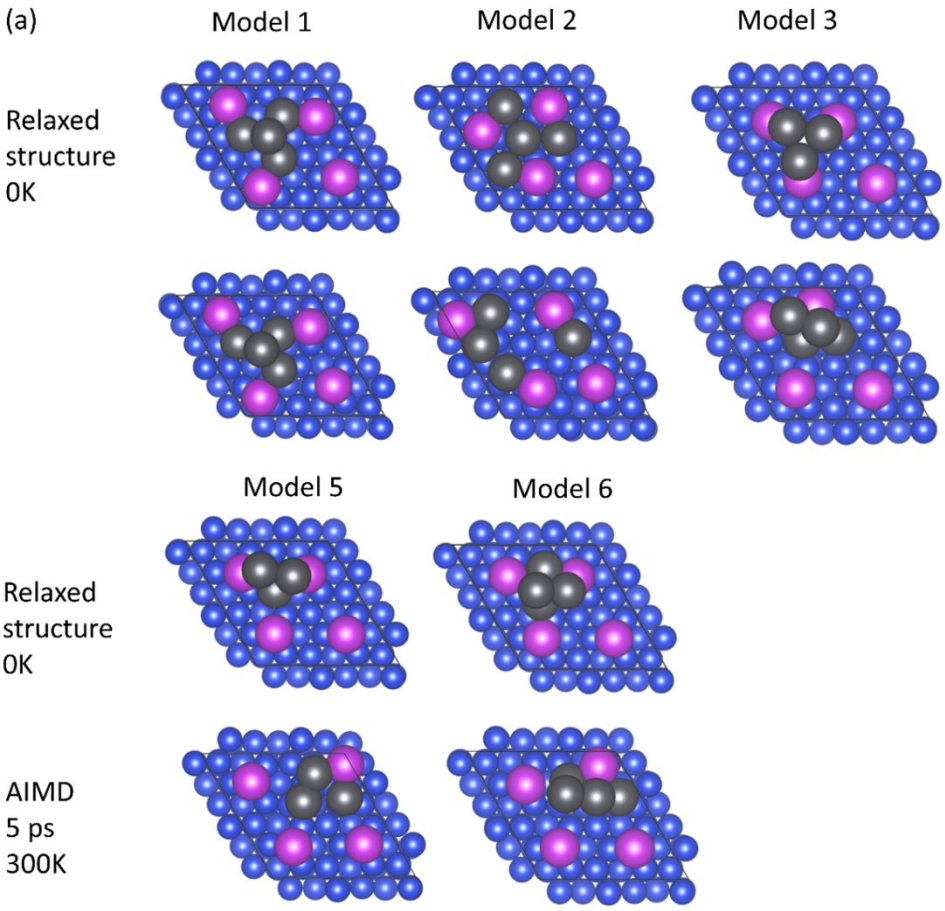

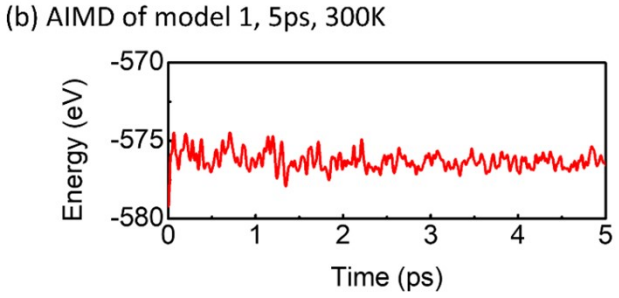

Figure S6. AIMD for models 1~3 at room temperature (300K) for 5 ps (5000 steps, 1 fs per step). Only model 1 remains the initial structure which is the one being used in the whole paper. The energy change regarding time for model 1 is shown in S6(b) where a stable energy flow can be observed. During AIMD lower Pb atoms moved in-plane. Once the distance between two Pb atoms was smaller than 3.15 Å they would repel and move against each other. Overall the structure remained unchanged.

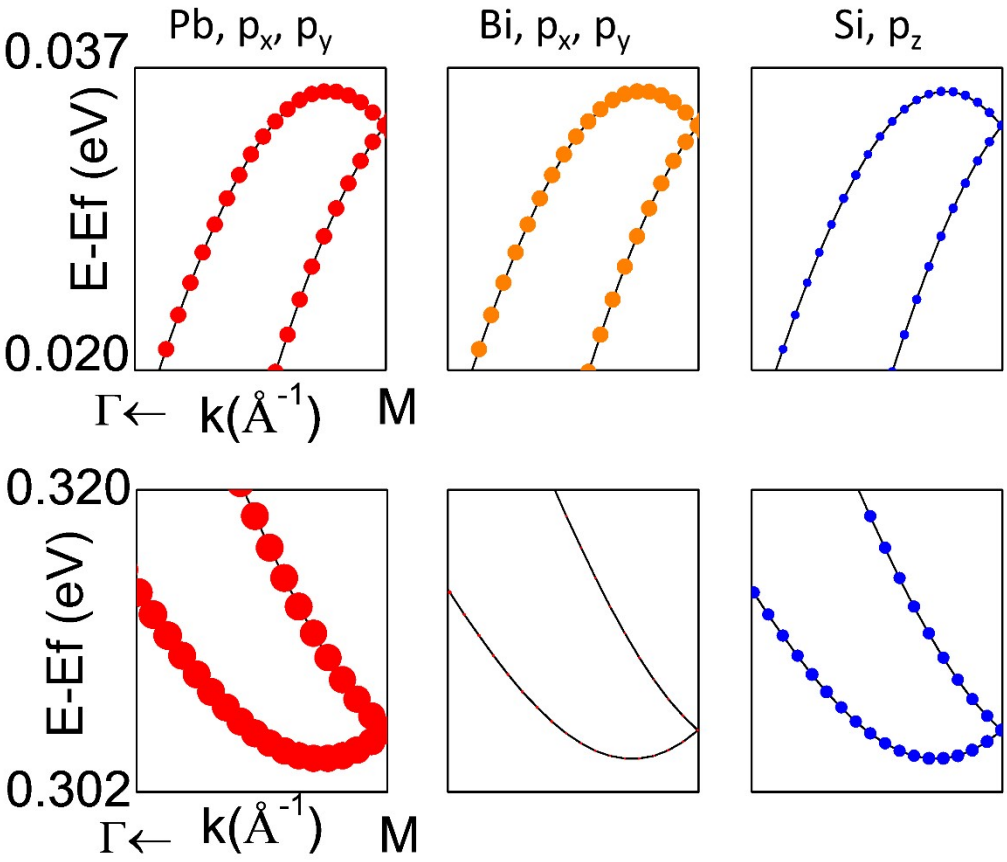

Figure S7. Orbital contributions to bands. The top row corresponds to bands in Figure 3(d) and the bottom row to Figure 3(e). The first, second, third columns correspond to contribution from Pb p_x (p_y) orbitals, Bi p_x (p_y) orbitals, Si p_z orbitals, respectively. Symbol sizes represent the corresponding orbital proportion. For the top band, Bi Pb p_x (p_y) orbitals provide primary contribution due to Pb-Bi bonds, while Si p_z orbitals contribute about half to that of Pb and Bi. For the bottom band, Pb p_x (p_y) orbitals dominate followed by Si p_z orbitals (around one-third to Pb proportion) because of formation of Pb-Si bonds and Pb-Pb bonds.

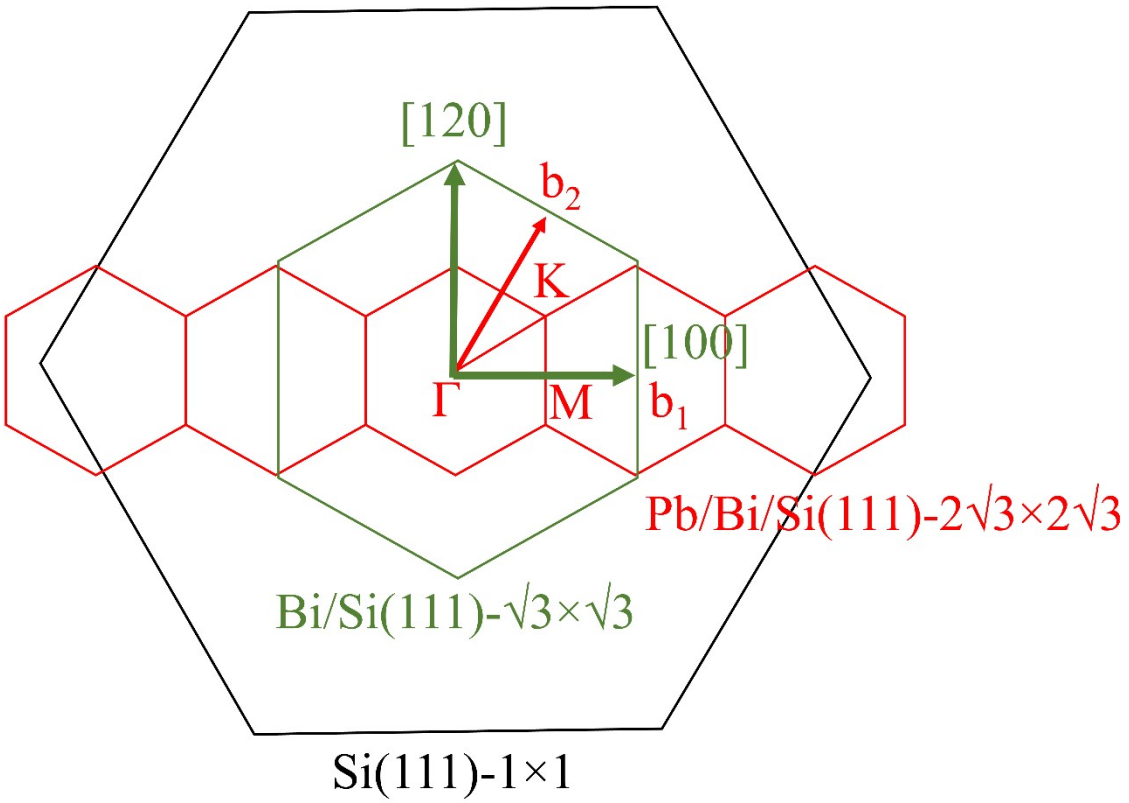

Figure S8. Brillouin zone of the superlattices. The biggest black hexagon corresponds to Si(111)-1×1 lattice. The smaller green hexagon is α-phase Bi √3×√3 lattice, which is 30° rotated with regard to Si(111). The smallest red hexagon is the 2√3×2√3 Pb phase, which is aligned with the Bi Brillouin zone. The [100] and [120] directions in the heterostructure mentioned in Figures 3(i) and S9 have been labeled by the green arrows. Those two directions correspond to M and K points in the Brillouin zone, respectively, where the former exhibits Rashba spin splitting.

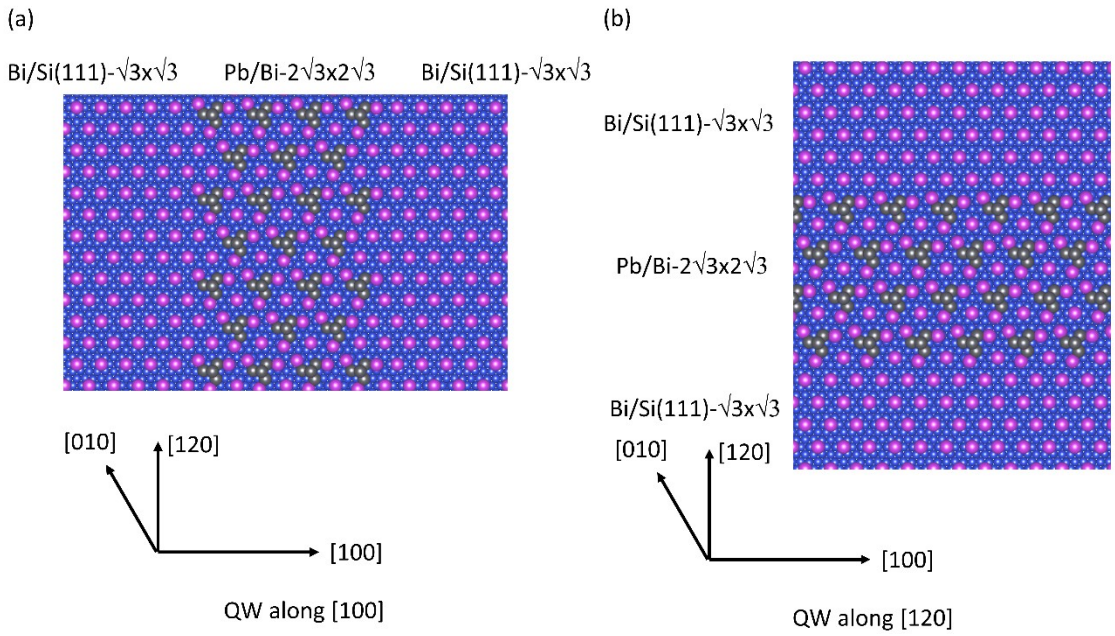

Figure S9. Top view of the α-Bi/2√3×2√3/α-Bi quantum well (QW) structures along (a) [100] direction and (b) [120] direction, respectively. Since [100] direction corresponds to M point in Brillouin zone, as shown in Figure S8, quantum well states along this direction will also exhibit Rashba spin splitting same as that in 2√3×2√3 superlattices. However, [120] direction matches K point in Brillouin zone which will fail in prominent spin splitting.

References

(1) Liboff, R. L., *Introductory Quantum Mechanics*. 4 ed.; Addison Wesley: San Francisco, 2003.

(2) Miwa, R. H.; Schmidt, T. M.; Srivastava, G. P., Bi covered Si(111) surface revisited. *J. Phys.: Condens. Matter* **2003,** *15* (17), 2441-2447.

(3) Liang, Q.-F.; Yu, R.; Zhou, J.; Hu, X., Topological states of non-Dirac electrons on a triangular lattice. *Physical Review B* **2016,** *93* (3).

(4) Rafiee, M.; Jalali Asadabadi, S., Quantum size effects in Pb/Si(111) thin films from density functional calculations. *Computational Materials Science* **2009,** *47* (2), 584-592.

(5) Giraud, S.; Wignacourt, J.-P.; Drache, M.; Nowogrocki, G.; Steinfink, H., The Stereochemical Effect of 6s2Lone-Pair Electrons: The Crystal Structure of a New Lead Bismuth Oxyphosphate Pb4BiO4PO4. *J. Solid State Chem.* **1999,** *142* (1), 80-88.

(6) Jain, A.; Ong, S. P.; Hautier, G.; Chen, W.; Richards, W. D.; Dacek, S.; Cholia, S.; Gunter, D.; Skinner, D.; Ceder, G.; Persson, K. a., The Materials Project: A materials genome approach to accelerating materials innovation. *APL Materials* **2013,** *1* (1), 011002.

(7) Ren, X.-Y.; Kim, H.-J.; Yi, S.; Jia, Y.; Cho, J.-H., Spin-orbit coupling effects on the stability of two competing structures in Pb/Si(111) and Pb/Ge(111). *Physical Review B* **2016,** *94* (7).

(8) Noffsinger, J.; Cohen, M. L., Superconductivity in monolayer Pb on Si(111) from first principles. *Solid State Commun.* **2011,** *151* (6), 421-424.

(9) Bychkov, Y. A.; Rashba, E. I., Properties of a 2D electron gas with lifted spectral degeneracy. *Soviet Journal of Experimental and Theoretical Physics Letters* **1984,** *39* (2), 4.